Electronic Supplementary Material (ESI) for Journal of Materials Chemistry A.

Supporting Information

Decorating nanoporous ZIF67-derived $NiCo_2O_4$ shell on Co_3O_4 nanowire array core for battery-type electrodes with enhanced energy storage performance

Dongbo Yu,[a] Bin Wu,[a] Liang Ge,[a] Liang Wu,[a] Huanting Wang[b] and Tongwen Xu*[a]

[a] *CAS Key Laboratory of Soft Matter Chemistry, Collaborative Innovation Center of Chemistry for Energy Materials, School of Chemistry and Material Science, University of Science and Technology of China, Hefei 230026, People's Republic of China*

[b] *Department of Chemical Engineering, Monash University, Clayton, Victoria 3800, Australia*

**E-mail addresses: twxu@ustc.edu.cn*

Experimental Section

Synthesis of cobalt carbonate hydroxide nanowire array (Co-NA) supported on Ni foam

In a typical synthesis, Ni foam (2 cm*2 cm in rectangular shape) (surface mass density: 500 g/m^2; thickness: 2 mm. Suzhou jiashide metal foam Co., Ltd) was washed in 3 M HCl solution by ultrasonic for 60 min, following rinse with ethanol and water for several times. 0.6 g of $CoCl_2 \cdot 6H_2O$ and 1.89 g of urea were dissolved in 8 ml of water, and the mixed solution was transferred into a Teflon-lined stainless steel autoclave with a capacity of 40 ml and Ni foam was immersed into it. The top side of Ni foam was covered by a polytetrafluoroethylene tape to avoid the undesired deposition of by-product from reaction solution. Subsequently, the autoclave was sealed and heated at 90 °C for 12 h, then cooled to room temperature naturally. Finally, cobalt carbonate hydroxide nanowire array on Ni foam was prepared.

Synthesis of Co-NA@ZIF-67 core-shell nanowire array (Co-NA@ZIF-67)

The prepared Co-NA was reacted with 2-methylimidazole aqueous solution (5g in 20 ml water) in a sealed bottle at room temperature. After 24 h reaction, the color change from pink of Co-NA to violet of product could be observed, indicating the formation of ZIF-67. The resulting Co-NA@ZIF-67 was washed with ethanol and water, and then dried in a 70^{o}C oven overnight.

Thermal conversion of Co-NA@NiCo-OH LDH and Co-NA@Co-OH LDH core-shell nanowire array into Co-Co_3O_4@ZIF-Co_3O_4 and Co-Co_3O_4@ZIF-$NiCo_2O_4$ core-shell nanowire array

To convert the ZIF-67 shell of Co-NA@ZIF-67 to NiCo-OH LDH and Co-OH LDH**,** Co-NA@ZIF-67 was simply immersed into 0.2 M $Ni(NO_3)_2$ and $Co(NO_3)_2$ methanol solution, the transformation proceeded at room temperature lasting for 24 h, the violet color vanished. The as-synthesized Co-NA@NiCo-OH LDH and Co-NA@Co-OH LDH were subsequently annealed at 300°C in air for 3 h at a heating rate of 2 ^{o}C/min, Co-NA core, Co-OH LDH shell and NiCo-OH LDH shell were decomposed to Co_3O_4 and $NiCo_2O_4$ oxides finally. For comparison, the thermal conversion from Co_3O_4@ZIF-67 core-shell nanowire array to Co_3O_4@ZIF-67-derived Co_3O_4 hybrid nanowire array (Co_3O_4@ZIF-Co_3O_4) was also carried out, as illustrated in Scheme S1. By heating the cobalt carbonate hydroxide nanowire array precursor at 300°C for 3h in air, Co_3O_4 nanowire array on Ni foam was synthesized, which was immersed into $Co(NO_3)_2$ methanol solution for 0.5 h, and then 2-methylimidazole methanol solution was added into the solution, the Co_3O_4 nanowire array served as the template to direct the crystallization of ZIF-67 shell, structured Co_3O_4@ZIF-67 core-shell nanowire array (Co_3O_4@ZIF-67) was prepared. Annealing Co_3O_4@ZIF-67 in air, Co_3O_4@ZIF-Co_3O_4 was obtained, and the annealing procedure is the same as that of the above Co-Co_3O_4@ZIF-$NiCo_2O_4$. The mass of pristine Co-NA-derived Co-Co_3O_4, Co_3O_4@ZIF-Co_3O_4, Co-Co_3O_4@ZIF-Co_3O_4 and Co-Co_3O_4@ZIF-$NiCo_2O_4$ was measured by calculating the increased mass of Ni foam, their mass loading was determined as 4.0, 4.8, 4.5 and 4.6 mg/cm^2, repectively.

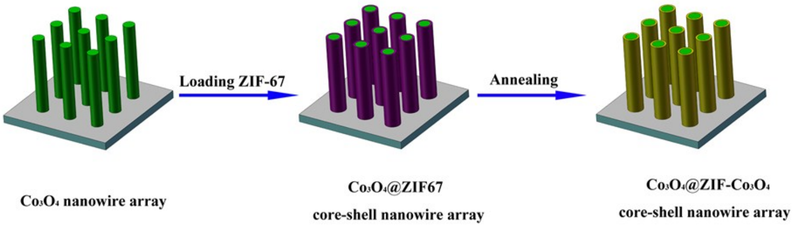

Scheme S1 Schematic illustration of the fabrication process for Co_3O_4@ZIF-Co_3O_4 core-shell nanowire array electrode on Ni foam.

Materials characterizations and electrochemical measurements

The X-ray diffraction (XRD) analysis was conducted on a Rigaku D/MAX2500VL/PC X-ray diffractometer with Cu Kα radiation. The structure and component information of the materials was got through a field-emission scanning electron microscopy (SEM, SU8020) and a transmission electron microscopy (TEM, JEM-2100) operated at 200 KV. The as-prepared samples were first treated in a strong ultrasonic bath for ~ 30 seconds (TJS-3000 Intelligent Ultrasonic Generator V6.0) to collect the pure black powders, which was dried at 80°C. The collected sample powders were then analyzed by the nitrogen sorption technique using a Micromeritics

ASAP 2020 instrument at 77 K, the surface area values were calculated by using the Brunauer-Emmett-Teller (BET) method in the relative pressure (P/P_o) range of 0.002-0.3. The X-ray photoelectron spectroscopy (XPS) analyses were examined on a Thermo Fisher X-ray photoelectron spectrometer system (ESCALAB250).

A three-electrode system was used to investigate the electrochemical performances in 6 M KOH electrolyte solution. 1 cm^2 of Ni foam with synthesized active materials was directly used as the working electrode, KCl saturated Ag/AgCl and Pt rod were respectively used as the reference electrode and the counter electrode. The electrochemical impedance spectroscopy (EIS) measurement was tested in the frequency range from 0.1Hz to 100 kHz at open-circuit potential with an ac perturbation of 0.1 V. The area capacity (C/cm^2) of the electrodes was calculated based on Equation 1 (CV plots) and Equation 2 (galvanostatic charge/discharge curves), and the specific capacity of the electrode was calculated by Equation 3:

$$\mathrm{C_a} = \frac{\int_{V_a}^{V_c} I(V)dV}{Sv} \qquad \text{Equation 1}$$

Where C_a is the area capacity (C/cm^2), S is the geometrical area of the electrode (cm^2) and ν is the scan rate of CV curves (V/s).

$$C_{\mathrm{a}} = \frac{I\Delta t}{S} \qquad \text{Equation 2}$$

Where C_a is the area capacity (C/cm^2), I is the discharge current (A), S is the geometrical area of the electrode (cm^2) and Δt is the total discharge time (s).

$$C_s = \frac{I\Delta t}{m} \qquad \text{Equation 3}$$

Where C_s is the specific capacity (C/g), I is the discharge current (A), m is the mass of the active materials (g) and Δt is the total discharge time (s).

The asymmetric supercapacitor was assembled and measured in a two-electrode system. A piece of Co-Co_3O_4@ZIF-$NiCo_2O_4$ on Ni foam (1 cm * 1 cm) was cut and directly pressed onto another Ni foam (1 cm * 3 cm) as the positive electrode. For the preparation of negative electrode, 90 wt% of commercial active carbon (BET surface area: 2000±100 m^2/g; particle size: 5±1; pore volume: 0.8-1.0 cm^3/g; pore size: 2.0-2.2 nm. TF-B520, Shanghai Sino Tech Investment Management Co., Ltd) was mixed with 10 wt% PVDF in addition of NMP to make a slurry, the mixed slurry was then cast a 1 cm^2 of area on a Ni foam (1 cm * 3 cm), dried at 80°C for 12 h and pressed under 10 MPa pressure. The two electrodes and a cellulose separator permeable to ion transport were placed into a test fixture consisting of two stainless steel plates, with 6 M KOH aqueous solution as the electrolyte. All the electrochemical measurements were carried out with an Autolab 3 electrochemical workstation. The specific capacitance (C, F/g), specific energy density (SE, Wh/kg) and specific power density (SP, W/kg) were calculated from chronopotentiometric curves using following Equation 4-6, respectively.

$$\mathrm{C} = \frac{I\Delta t}{m'\Delta V} \qquad \text{Equation 4}$$

Where C is the specific capacitance (F/g), I is the discharge current (A), m is the total mass of both positive and negative electrodes (g), Δt is the discharge time (s) and ΔV is the window potential during the discharge process.

$$SE = \frac{C\Delta V^2}{7.2} \qquad \text{Equation 5}$$

Where SE is the specific energy density (Wh/kg), C is the specific capacitance (F/g), ΔV is the window potential during the discharge process.

$$SP = \frac{3600 * SE}{\Delta t} \qquad \text{Equation 6}$$

Where SP is the specific power density (W/kg), SE is the specific energy density (Wh/kg) and Δt is the discharge time (s).

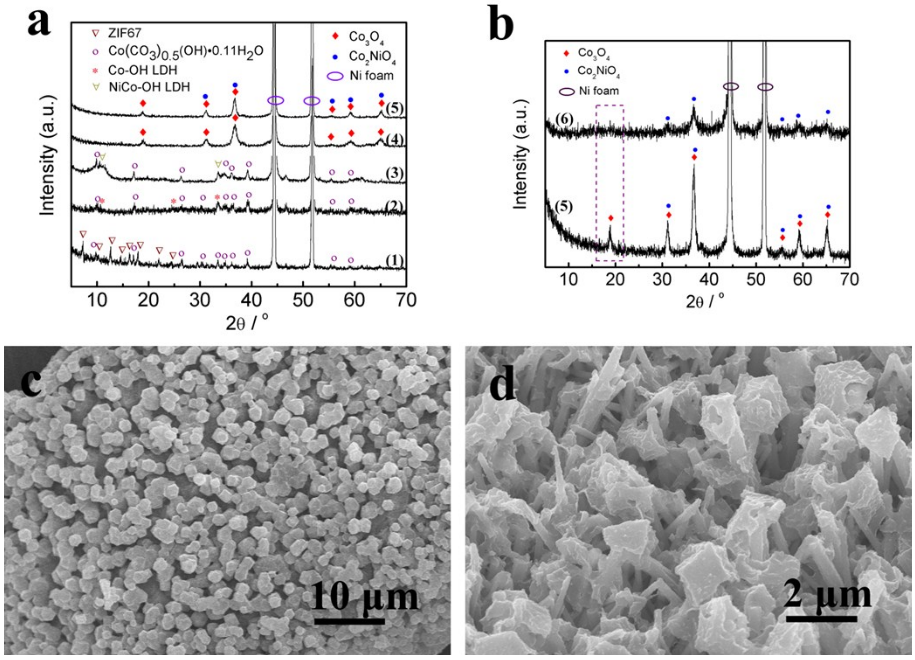

Figure S1 (a) XRD patterns of the products at every step: (1) Co@ZIF67, (2) Co@Co-OH, (3) Co@NiCo-OH, (4) Co-Co_3O_4@ZIF-Co_3O_4 and (5) Co-Co_3O_4@ZIF-$NiCo_2O_4$; (b) XRD of Co-Co_3O_4@ZIF-$NiCo_2O_4$ by using the precursor Co@ZIF67 at 5-day reaction at room temperature (6); SEM images of the precursor Co@ZIF67 at 36 h reaction (c) and its resulting product of Co-Co_3O_4@ZIF-$NiCo_2O_4$ (d). When cobalt carbonate hydroxide nanowire array was reacted with 2-methylimidazole for a long time, it could be seen a layer of dispersive ZIF67 particles (2 ~ 3 μm) covering on the top of nanowire array (Figure S1c); after completing the conversion from ZIF67 to layer double hydroxide NiCo-OH and post-annealing treatment, some of ZIF67 particle-derived particles still retained because of their strong adhesion force to nanowire array (Figure S1d). It was clear to observe the peak located at ~19^{o} of its XRD pattern (this peak corresponds to Co_3O_4, the other peak locations of Co_3O_4 are almost the same as those of $NiCo_2O_4$) disappeared (Figure S1b Curve 6), implying the amount of $NiCo_2O_4$ is much larger than Co_3O_4 and Co_3O_4 had not been detected; integrated with the following core-shell morphology from SEM and TEM characterizations, it thus could be concluded that $NiCo_2O_4$ was actually converted from ZIF67, and Co-Co_3O_4@ZIF-$NiCo_2O_4$ of the Curve 5 was composed of two mixed phases: $NiCo_2O_4$ and Co_3O_4.

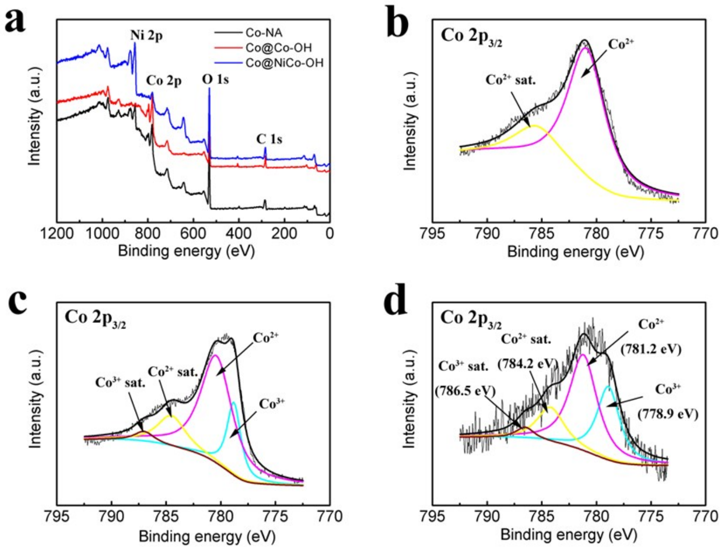

Figure S2 XPS full spectra of Co-NA, Co@Co-OH and Co@NiCo-OH (a), high-resolution XPS spectra of Co $2p_{3/2}$: Co-NA (b), Co@Co-OH (c) and Co@NiCo-OH (d). Compared with Co-NA, it is obvious to see two new peaks located at 778.9 eV and 786.5 eV appear for Co@Co-OH and Co@NiCo-OH, which can be associated to Co^{3+} and Co^{3+} satellite peak. The coexistence of Co^{3+} and Co^{2+} reveals the formation of layered double hydroxides, agreeing with the XRD observation.

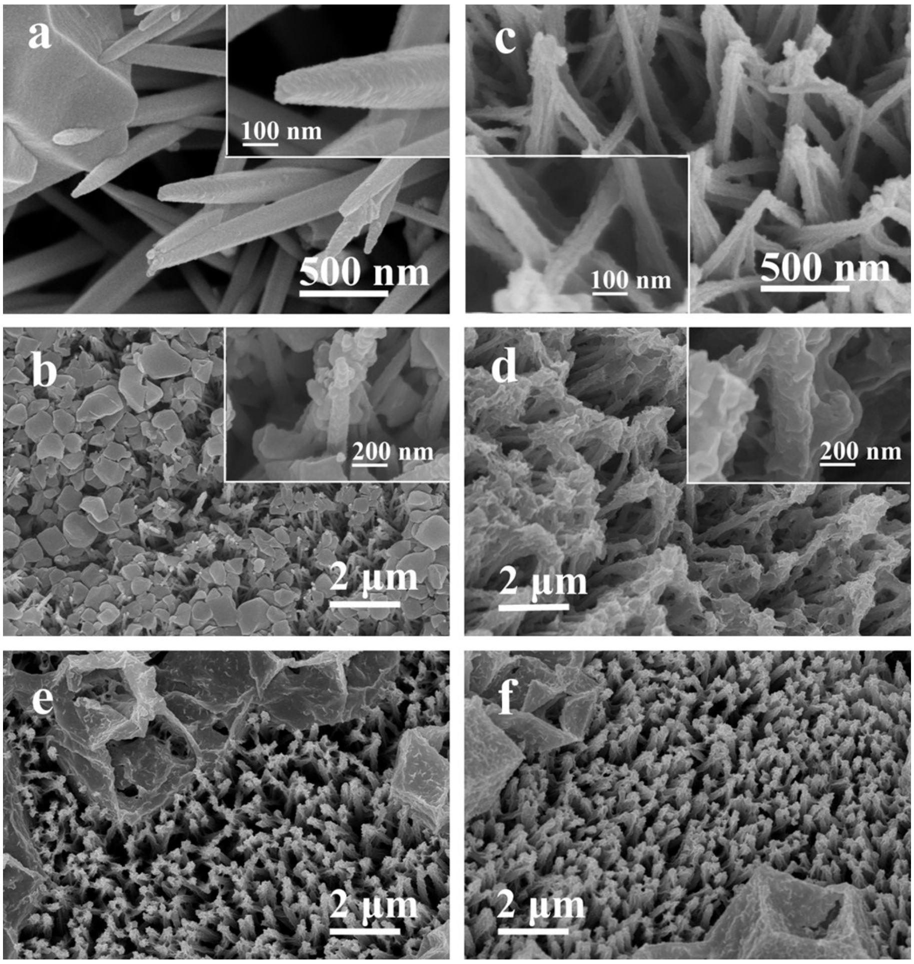

Figure S3 SEM images of Co-NAs in 2-methylimidazole aqueous solution for 12 h (a) and 36 (b). SEM images of resulting Co@NiCo-OH after further placing Co@ZIF67 (at different reaction time) in 0.2 M $Ni(NO_3)_2$ methanol solution for another 24 h: at 12 h (c), 36 h (d) and 24 h (e, f).

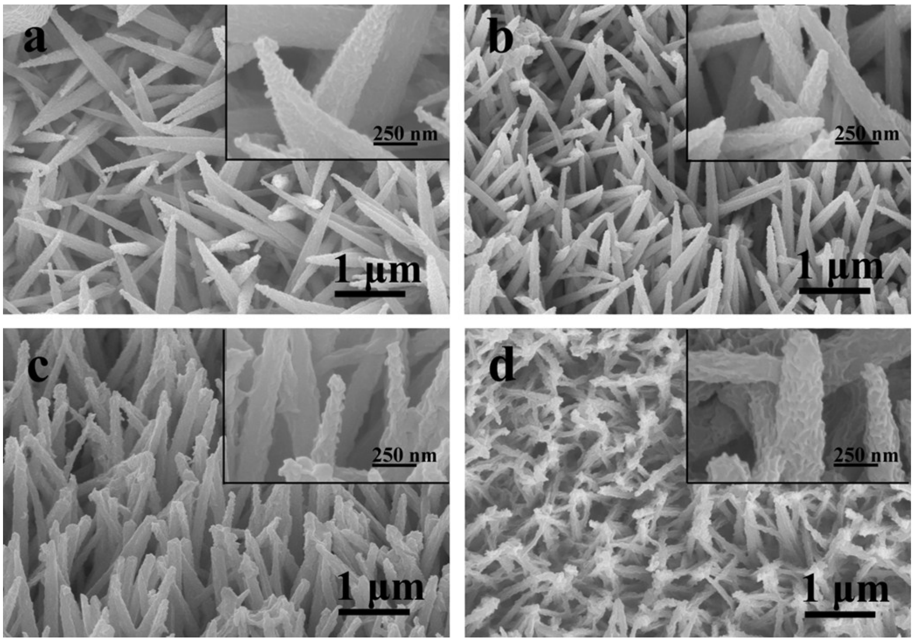

Figure S4 SEM images of resulting Co@NiCo-OH in $Ni(NO_3)_2$ methanol solution at different concentration: 0.05 M (a), 0.1 M (b), 0.15 M (c) and 0.2 M (d).

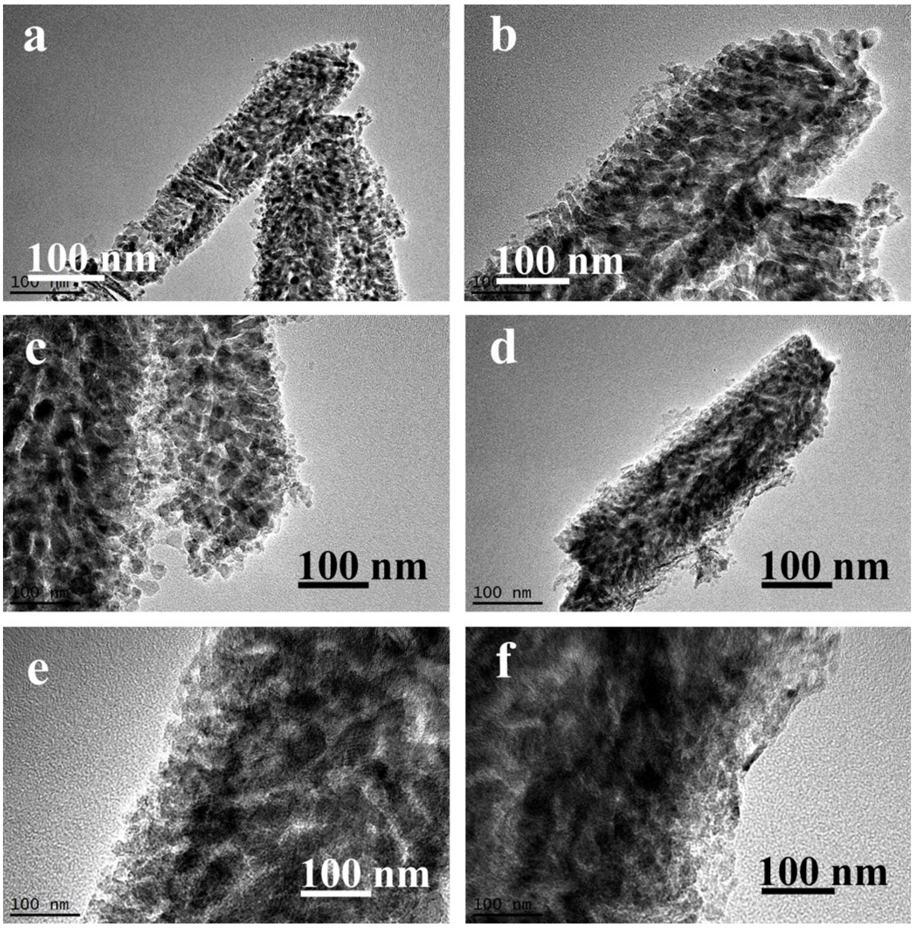

Figure S5 TEM images of Co-Co_3O_4@ZIF-$NiCo_2O_4$. We could identify the different particle size of the core and the shell, because NiCo-OH LDH-derived Co_3O_4 (5~15 nm) achieved smaller size than cobalt carbonate hydroxide-derived one (40 ~ 50 nm).

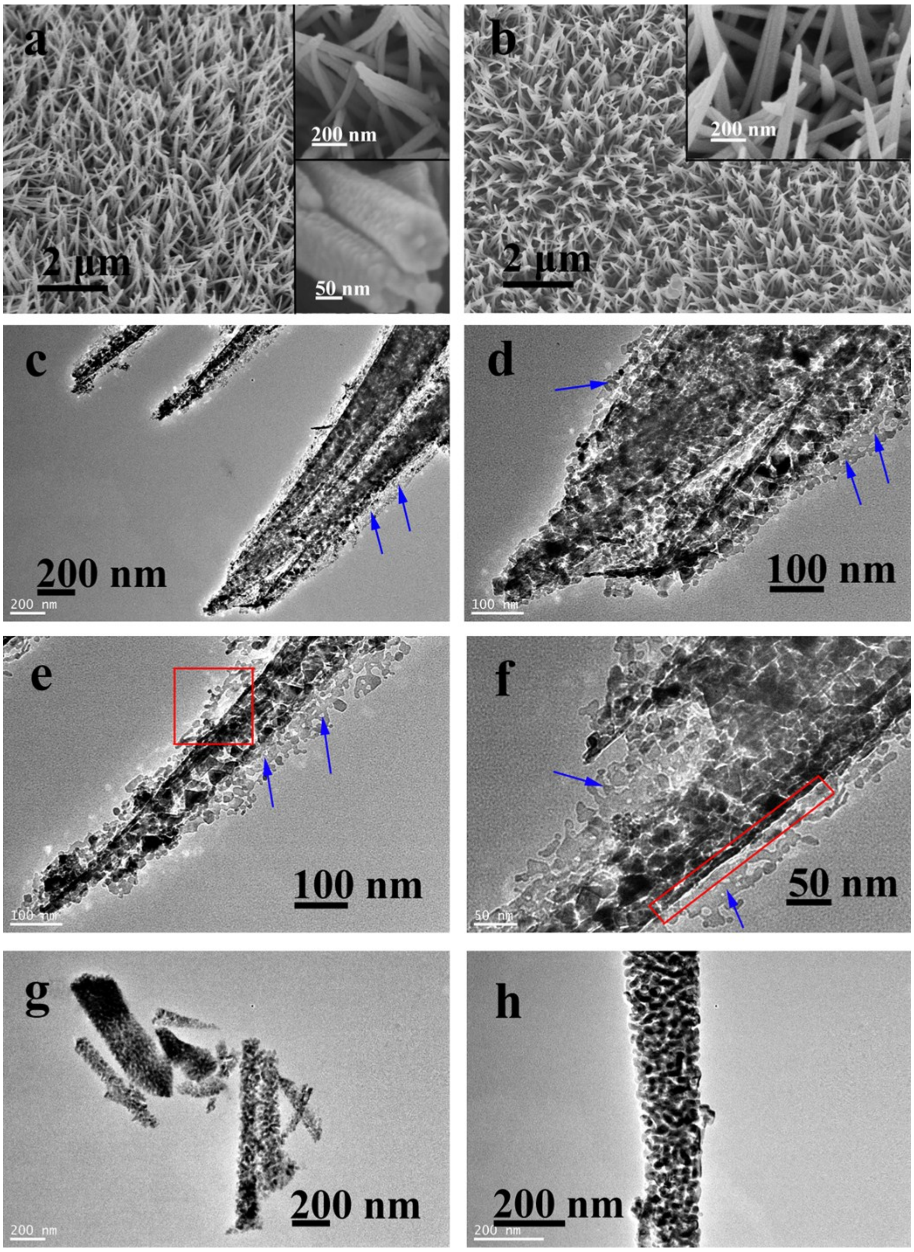

Figure S6 SEM images of Co_3O_4@ZIF67 (a) and Co_3O_4@ZIF-Co_3O_4 (b); TEM images of Co_3O_4@ZIF-Co_3O_4 (c-h). We could clearly see the ZIF67 shell were successfully grown on Co_3O_4 nanowire core (a); it seemed like there was no structure change after heating at 300°C according to SEM observation (a, b), but TEM images revealed ZIF67-derived Co_3O_4 shell presented thin nanoflake morphology rather than nanoparticle (blue arrows in c-f), unsatisfying phase separation occurred (red rectangle areas in e, f), which may be attributed to the different volume shrinkage of ZIF67 and Co_3O_4 in annealing process; desperately, some of nanoflake shells were even peeled away from the nanowire core, no core-shell structure remained (g, h).

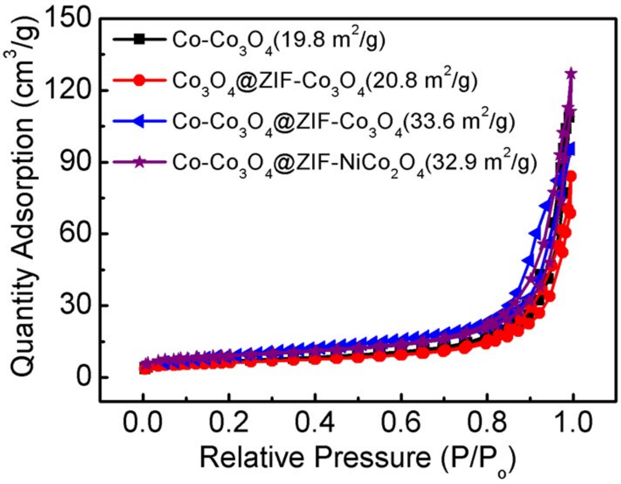

Figure S7 Nitrogen adsorption–desorption isotherms of pristine Co-Co_3O_4, Co_3O_4@ZIF-Co_3O_4, Co-Co_3O_4@ZIF-Co_3O_4 and Co-Co_3O_4@ZIF-$NiCo_2O_4$.

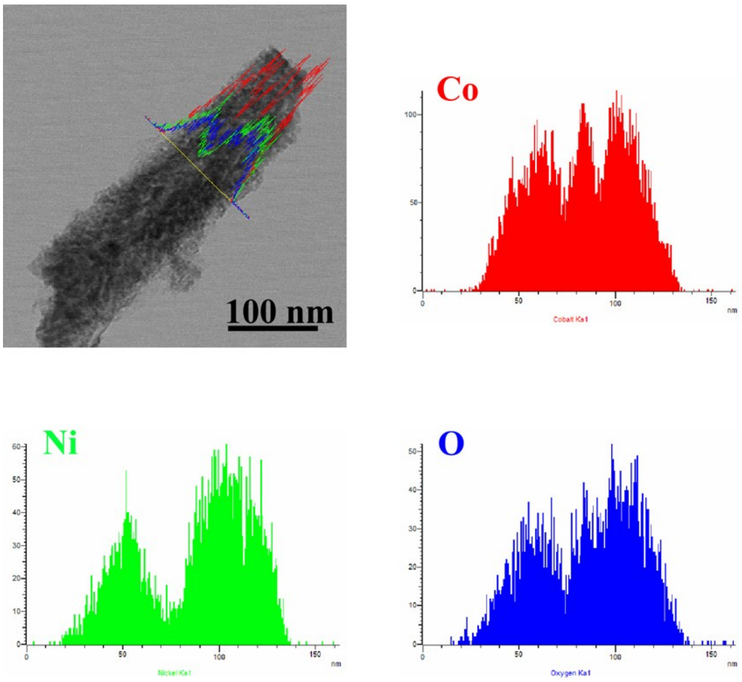

Figure S8 EDX line scan of a single Co-Co_3O_4@ZIF-$NiCo_2O_4$ core-shell hybrid nanowire. The ZIF67-derievd $NiCo_2O_4$ shell tightly enwrapped on the Co-Co_3O_4 core, no phase separation was observed between the shell and the core, indicating the perfect core-shell architecture of Co-Co_3O_4@ZIF-$NiCo_2O_4$.

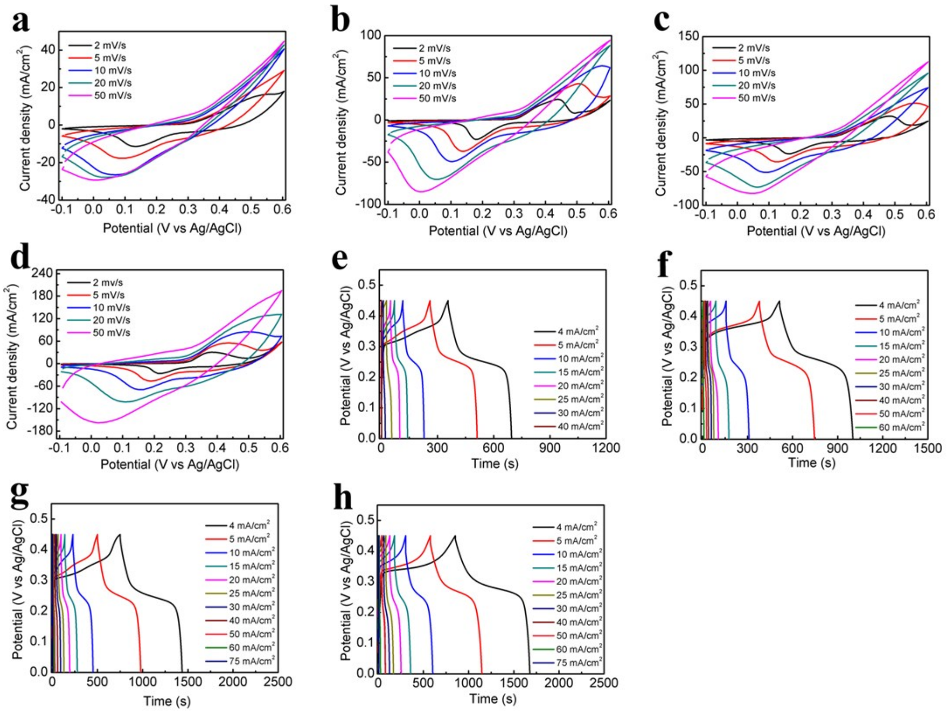

Figure S9 CV plots of Co-Co_3O_4 (a), Co_3O_4@ZIF-Co_3O_4 (b), Co-Co_3O_4@ZIF-Co_3O_4 (c) and Co-Co_3O_4@ZIF-$NiCo_2O_4$ (d) at the scan rate of 2, 5, 10, 20 and 50 mV/s; galvanostatic charge-discharge curves of Co-Co_3O_4 (e), Co_3O_4@ZIF-Co_3O_4 (f), Co-Co_3O_4@ZIF-Co_3O_4 (g) and Co-Co_3O_4@ZIF-$NiCo_2O_4$ (h) at different current density.

Table S1 Capacitance values of the electrodes extracted from Figure S9e-h

electrodes	**capacitance at 4 mA/cm^2**	**capacitance at 40 mA/cm^2**	**absolute capacitance loss**	**percentage of capacitance loss**
Co-Co$_3$O$_4$	1.35 C/cm^2	0.53 C/cm^2	0.82 C/cm^2	60.7 %
Co$_3$O$_4$@ZIF-Co$_3$O$_4$	1.97 C/cm^2	0.85 C/cm^2	1.12 C/cm^2	56.8 %
Co-C$_3$O$_4$@ZIF-Co$_3$O$_4$	2.82 C/cm^2	1.61 C/cm^2	1.21 C/cm^2	42.9 %
Co-Co$_3$O$_4$@ZIF-NiCo$_2$O$_4$	3.37 C/cm^2	2.11 C/cm^2	1.26 C/cm^2	37.4 %

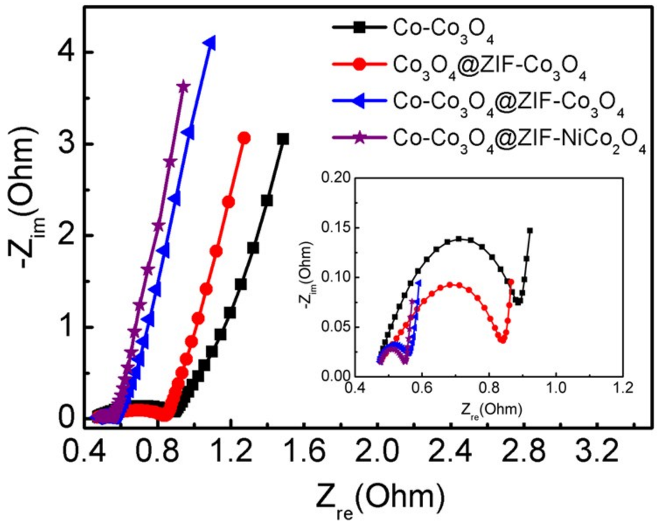

Figure S10 Nyquist plots of Co-Co$_3$O$_4$, Co$_3$O$_4$@ZIF-Co$_3$O$_4$, Co-Co$_3$O$_4$@ZIF-Co$_3$O$_4$ and Co-Co$_3$O$_4$@ZIF-NiCo$_2$O$_4$ at a range of 0.1 Hz ~100 kHz.

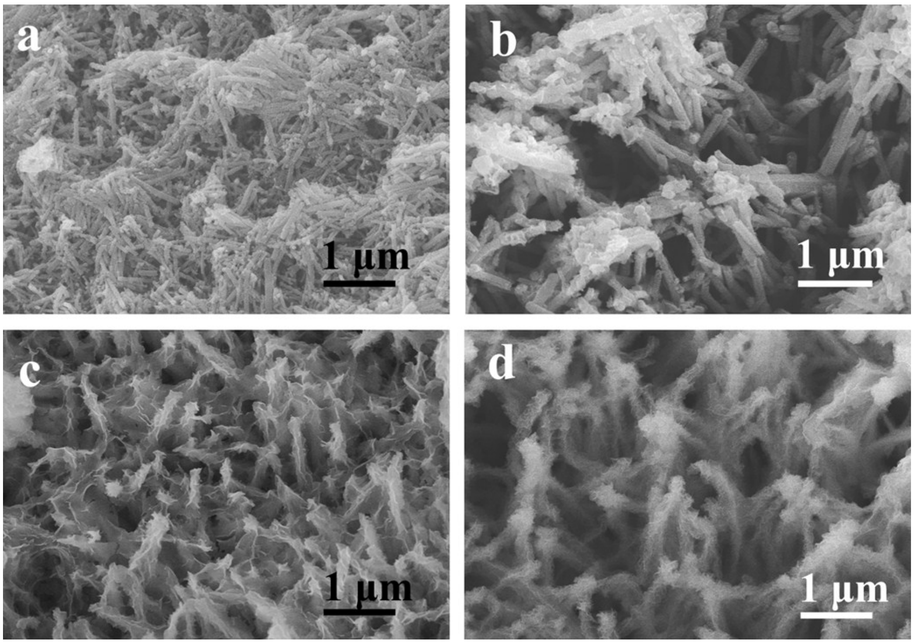

Figure S11 The resulting SEM images of Co-Co_3O_4 (a), Co_3O_4@ZIF-Co_3O_4 (b), Co-Co_3O_4@ZIF-Co_3O_4 (c) and Co-Co_3O_4@ZIF-$NiCo_2O_4$ (d) at the current density of 30 mA/cm^2 after 5000 cycles.

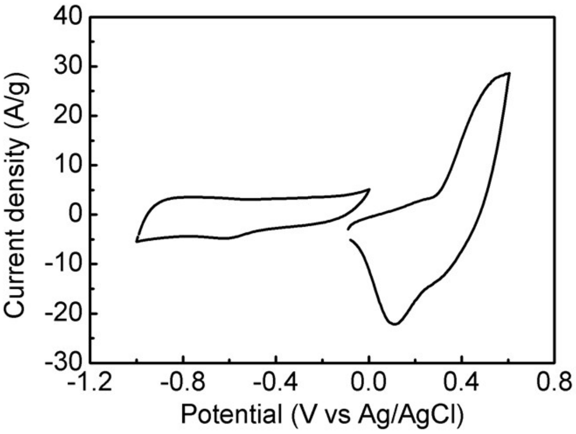

Figure S12 CV plots of positive electrode Co-Co_3O_4@ZIF-$NiCo_2O_4$ (+) and negative electrode AC (-) at a scan rate of 20 mV/s. As for a full supercapacitor cell, the charge balance followed the relationship $Q_+ = Q_-$. The charge stored by electrodes depended on specific capacitance (C), potential range for the charge/discharge process (ΔE) and the mass of the electrode (m), and the charge could be describe as: $Q = C * m * \Delta E$, so the mass balancing of Co-Co_3O_4@ZIF-$NiCo_2O_4$/AC (m_+/m_-) was calculated as:

$$\frac{m_+}{m_-} = \frac{C_- * \Delta E_-}{C_+ * \Delta E_+} = \frac{151 * 1}{456 * 0.7} = 0.473 .$$

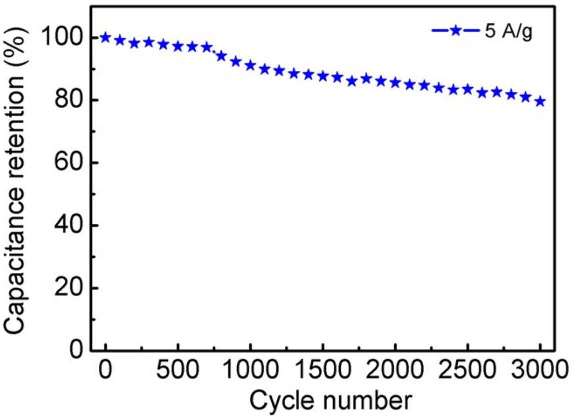

Figure S13 Cycling stability of the assembled asymmetric supercapacitor Co-Co_3O_4@ZIF-$NiCo_2O_4$//AC measured at a current density of 5 A/g.